Residual Diagnosis of Diabatic Heating from ERA-40 and NCEP Reanalyses: Intercomparisons with TRMM

STEVEN C. CHAN AND SUMANT NIGAM

Department of Atmospheric and Oceanic Science, University of Maryland, College Park, College Park, Maryland

(Manuscript received 8 January 2008, in final form 29 April 2008)

ABSTRACT

Diabatic heating is diagnosed from the 40-yr ECMWF Re-Analysis (ERA-40) circulation as a residue in the thermodynamic equation. The heating distribution is compared with the heating structure diagnosed from NCEP and 15-yr ECMWF Re-Analysis (ERA-15) circulation and latent heating generated from Tropical Rainfall Measuring Mission (TRMM) observations using the convective–stratiform heating (CSH) algorithm.

The ERA-40 residual heating in the tropics is found to be stronger than NCEP's (and ERA-15), especially in July when its zonal–vertical average is twice as large. The bias is strongest over the Maritime Continent in January and over the eastern basins and Africa in July. Comparisons with precipitation indicate ERA-40 heating to be much more realistic over the eastern Pacific but excessive over the Maritime Continent, by at least 20% in January.

Intercomparison of precipitation estimates from heating-profile integrals and station and satellite analyses reveals the TRMM CSH latent heating to be chronically weak by as much as a factor of 2! It is the low-side outlier among nine precipitation estimates in three of the four analyzed regions. No less worrisome is the inconsistency between the integral of the CSH latent heating profile in the tropics and the TRMM precipitation retrievals constraining the CSH algorithm (e.g., the 3A25 analysis).

Confronting TRMM's diagnosis of latent heating from *local* rainfall retrievals and *local* cumulus-model heating profiles with heating based on the *large-scale* assimilated circulation is a defining attribute of this study.

1. Introduction

The earth's atmosphere is primarily heated from below by the sensible, latent, and radiative (longwave) heat fluxes originating at the land surface. Related flux divergence and water phase change leads to diabatic heating of the atmosphere. Atmospheric circulation arises in response to the horizontal and vertical variations of heating and their influence on temperature and, in turn, modulates diabatic heating itself through impact on the heat fluxes. The diabatic heating distribution and the general circulation of the atmosphere are thus strongly linked. Diabatic heating is, however, an elusive quantity, observationally. The elusiveness stems from it being related to both local and advective changes, and that too of potential temperature rather than ordinary temperature, which can at least be measured. The diagnosis of potential temperature change, moreover, involves the vertical velocity, which is measurable in principle but not in practice on account of its extreme smallness at synoptic scales.

Diabatic heating is thus diagnosed from the atmospheric circulation (winds, temperature), usually through the thermodynamic equation (e.g., Holopainen and Fortelius 1986; Hoskins et al. 1989) in which diabatic heating appears explicitly. The residual estimation is, however, prone to errors in view of the uncertainties in diagnosis of the pressure vertical velocity (ω), especially from uninitialized atmospheric data. Modern retrospective analysis (i.e., reanalysis) of global atmospheric circulation produced at the National Centers for Environmental Prediction (NCEP) (Kalnay et al. 1996) and, more recently, at the European Centre for Medium-Range Weather Forecasts (ECMWF) (Uppala et al. 2005) with improved forecast models and data assimilation strategies, yield more consistent ω estimates dynamically, thermodynamically, and mass-balance-wise, enhancing prospects of obtaining a refined distribution of diabatic heating for at least the recent decades.

A refined description of the heating structure is needed for improving the physical parameterizations in atmospheric models. Modeling of atmospheric convection,

Corresponding author address: Sumant Nigam, 3419 Computer and Space Sciences Bldg., University of Maryland, College Park, College Park, MD 20742-2425.
E-mail: nigam@atmos.umd.edu

DOI: 10.1175/2008JCLI2417.1

especially partitioning between convective and stratiform processes, remains a formidable challenge. The partitioning is as consequential for atmosphere–land surface interactions in the subtropics as it is for atmosphere–ocean interaction in the deep tropics. In both cases, the diabatic heating profile in the lower troposphere exerts profound influence on the low-level circulation, planetary boundary layer structure, and surface fluxes—albeit in different ways given the different thermodynamic balance in the regions. The considerable influence of the heating profile on the upper-troposphere circulation is well documented (e.g., Ting and Sardeshmukh 1993; Schumacher et al. 2004).

A refined description of the circulation-consistent heating vertical structure can, perhaps, spur development of convection algorithms, alleviating current model shortcomings such as lack of stratiform precipitation and attendant overproduction of convective rain. The resulting bias in the convective–stratiform precipitation ratio can lead to bottom-heavy heating profiles in the tropics (e.g., Houze 1997; Nigam et al. 2000) and spurious heating of the lower troposphere in the subtropics/midlatitudes that can lead to unwanted feedbacks, including precipitation recycling in the warm season.

Given the importance of the heating distribution in advancing understanding and modeling of the atmospheric general circulation, and the error-prone residual estimation of heating, it is surprising that diabatic heating data are not part of the publicly accessible ECMWF reanalysis archives [15- or 40-yr ECMWF Re-Analyses (ERA-15 or ERA-40)]. The field is, of course, generated during the reanalysis cycle, as part of the short-term bridging forecast, initiated from the reanalysis circulation. The ERA-40 atlas (Kållberg et al. 2005) does display the heating obtained in this manner, both in column-integrated and pressure-layer average formats. Diabatic heating generated during 6-h forecasts initiated with NCEP reanalysis circulation has been available for sometime, both in total and partitioned forms from the National Center for Atmospheric Research (NCAR) data archives.

The diagnosed heating vertical structure cannot be easily validated as diabatic heating is not an observable quantity. But the correspondence between vertically averaged heating and observed precipitation can provide an assessment of the residual diagnosis, at least in the deep tropics where latent heating is dominant. Note that the correspondence is not assured in the heating fields diagnosed from the NCEP and ERA global reanalysis, as the latter do not assimilate precipitation. Precipitation (diabatic heating) produced during the short-term bridging forecast of the reanalysis cycle—the archived precipitation—is impacted only by circulation observations and the model physical parameterizations in these datasets. Not surprisingly, both NCEP and ERA precipitation often exhibit substantial departures from the observed distribution.[1] Residually diagnosed heating—the focus of this paper—thus seems preferable to the one generated in the bridging forecasts, especially if precipitation observations are not assimilated, as is the case in current global reanalyses.[2]

The recent availability of the Tropical Rainfall Measuring Mission (TRMM) surface convective and stratiform rain rates, and related latent heating profiles based on cloud-resolving model analysis (Tao et al. 2001), raise prospects for validation of heating vertical structure in the tropics. Intercomparison of the profiles over continental and oceanic regions of intense precipitation in the tropics is a notable feature of this paper. Here TRMM profiles serve as a useful reference but not necessarily the validation target, in view of their own model (cloud ensemble) origin. The comparisons, in fact, provide useful reading on the amplitude of the TRMM latent heating profiles, especially in regions of adequate surface rainfall observations. To foster comparative analysis in other regions and seasons, the 3D diabatic heating diagnosed from ERA-40, NCEP, and ERA-15 global reanalyses is publicly distributed in isobaric coordinates (at monthly resolution) from the authors' department data server (http://dsrs.atmos.umd.edu/DATA/NIGAM/Diab.Heating/).

The datasets are briefly described in section 2 and the residual diagnosis of heating in section 3. Heating intercomparisons follow in section 4, which focuses on the zonal and vertical averages and the Hadley and Walker circulations and related heating distributions. Section 5 compares the evolution of vertically averaged heating against precipitation in regions where latent heating is dominant to assess the reasonableness of ERA-40 and NCEP heating. Section 6 focuses on the heating vertical structure, especially intercomparisons with TRMM, in the ITCZ and four selected continental and oceanic regions of intense precipitation: Indian summer monsoon, Maritime Continent, South American continent, and the Pacific winter storm tracks. Concluding remarks follow in section 7.

2. Datasets

a. ERA-40

The ERA-40 reanalysis (Uppala et al. 2005) is the ECMWF state-of-the-art global reanalysis for the period from 1957 to 2002. Generated almost a decade after the

[1] Sparse sampling of the atmospheric circulation (winds, temperature, humidity, etc.) in the tropics, especially over oceanic regions, also contributes to the precipitation departures, both directly and indirectly; the latter, by allowing the model biases and deficiencies to be more influential.

[2] Precipitation has been additionally assimilated in the recent North American Regional Reanalysis (Mesinger et al. 2006).

NCEP reanalysis (Kalnay et al. 1996), it benefits from recent advances is data assimilation and physical parameterizations and, of course, more complete historical datasets.

The reanalysis combines model forecast fields, radiosonde, and other in situ data including aircraft and ship reports and satellite data using a three-dimensional variational data assimilation (3DVAR) strategy. ERA-40 directly assimilates satellite-sounder radiances. The ERA-40 assimilating model (T159 with 60 vertical levels) is the modified ECMWF Integrated Forecasting System that was used in ECMWF operations between June 2001 and January 2002. The assimilating model uses the Tiedtke (1989, 1993) cumulus and large-scale precipitation parameterization schemes and updated land surface and PBL schemes. Additional details can be found at the ERA-40 Web site (http://www.ecmwf.int/research/era/do/get/era-40). The ERA-40 data were obtained from NCAR where the 6-hourly fields are archived on a 2.5° grid and 23 pressure levels.

Andersson et al. (2005) have shown that in the post-satellite-sounder period ERA-40 has a positive tropical moisture and precipitation bias, leading to hydrological imbalance with the annual-mean global $P - E$ being positive after 1973. Intercomparisons in this study also show the ERA-40 diagnosed heating to be excessive over the Maritime Continent.

b. ERA-15

ERA-15 is the predecessor of ERA-40, but for the period 1979–93 (Gibson et al. 1997). The initialized reanalysis was produced from intermittent statistical (optimum interpolation) analysis with 6-h cycling, one-dimensional variational physical retrieval of TIROS Operational Vertical Sounder cloud cleared radiances, and diabatic, nonlinear normal mode initialization of five vertical modes, using a T106 resolution (~120 km) spectral model with 31 vertical hybrid levels. Other model features include a prognostic cloud scheme and a mass flux convection scheme (Tiedtke 1989). More details can be found on the ERA-15 Web site (http://www.ecmwf.int/research/era/ERA-15/).

The ERA-15 reanalysis exhibits some artificial trends, arising from assimilation of satellite data (Trenberth et al. 2001). The related problem was fixed prior to the ERA-40 generation (Uppala et al. 2005). The ERA-15 data were obtained from NCAR where the 6-hourly fields are archived on a 2.5° × 2.5° global grid at 17 pressure levels.

c. NCEP reanalysis

The NCEP reanalysis (Kalnay et al. 1996) was produced from spectral statistical interpolation using a T62 resolution (~210 km) global spectral model with 28 vertical sigma levels; the model became operational in December 1994. The model uses a diagnostic scheme for clouds, and a simplified Arakawa–Schubert cumulus convection scheme (Pan and Wu 1994). A 3DVAR data assimilation scheme is employed and satellite soundings, rather than radiances, are assimilated. The 6-hourly fields are available on a 2.5° × 2.5° global grid at 17 pressure levels from January 1958. The pressure-level gridded geopotential, winds, temperature, and vertical velocity (ω) fields are generated from the leading T36 spectral amplitudes.

The diabatic heating generated during a 6-h model forecast starting from each timestep's reanalysis circulation is available, partitioned into six components: large-scale condensation, deep convective, shallow convective, longwave and shortwave radiation, and vertical diffusion heating rates. White and Saha (1996) document the vertical structure of the heating components and their variability during the 1982–93 period. However, in view of potential differences between the model-produced and the reanalysis-consistent heating (Ebisuzaki 1996), diabatic heating was residually diagnosed from the NCEP reanalysis circulation by Yanai and Tomita (1998) and Nigam et al. (2000).

d. NOAA/CPC Merged Analysis of Precipitation

The NOAA Climate Prediction Center (NOAA/CPC) merged analysis of monthly precipitation (CMAP) (Xie and Arkin 1996) is used to benchmark vertically averaged latent heating over the oceanic regions. Merged precipitation (on a 2.5° grid) was generated by combining gauge observations and satellite estimates derived from the infrared, outgoing longwave, and microwave scattering and emission-based precipitation indices. The Xie–Arkin dataset is short, beginning in January 1979, but global, and especially valuable over oceanic regions. The second version used here (CMAP-2) is not based on any input from the NCEP reanalysis.

e. TRMM precipitation

Three analyses of surface precipitation are used in this study: The first is the 3B43 analysis (on a 0.25°grid), which provides total monthly surface rainfall based on the TRMM Microwave Imager (TMI) and precipitation radar (PR), and ground station data. The second analysis (3A12)—an experimental one (on a 0.5°grid)—estimates monthly surface rainfall from the TMI, while the third one (3A25) estimates the near-surface monthly rainfall (on a 0.5°grid) from the PR.

f. Station precipitation

Precipitation from the Climate Research Unit's TS2.1 analysis of station data (Mitchell and Jones 2005) provides the monthly station precipitation estimate on a 0.5° grid over land regions. The recent 1.0° station precipitation analysis by the India Meteorological Department

(IMD) (Rajeevan et al. 2006) provides an additional rainfall estimate over the Indian subcontinent.

g. TRMM precipitation radar–based latent heating

The TRMM latent heating comes from the convective–stratiform heating (CSH) algorithm. The algorithm produces monthly latent heating profiles (up to 18 km in the vertical) at 0.5° horizontal resolution for the period beginning December 1997 (Tao et al. 1993, 2001). The algorithm is based on surface convective and stratiform rain rates as well as the type and location of observed cloud systems, identified using the precipitation radar. A lookup table provides stored convective and stratiform latent heating profiles for various types of cloud systems in different geographic locations; these profiles are obtained from simulations with the Goddard Space Flight Center cumulus ensemble model. The TRMM latent heating profiles are specified in geometric height coordinates from 500 m up to 18 km. The corresponding pressure-level profiles are obtained by linearly interpolating the geometric-height heating rates to the geopotential heights of the ERA-40 pressure levels, with the 1000-hPa specification needing extrapolation.

3. Residual diagnosis of diabatic heating

The 3D diabatic heating is diagnosed as a residual in the thermodynamic equation (e.g., Hoskins et al. 1989; Nigam 1994) using the analyzed vertical velocity (ω):

$$\overline{\dot{Q}}(x,y,p,t) = \frac{\Delta T}{\Delta t} + \overline{\mathbf{v}}\cdot\nabla\overline{T} + \left(\frac{p}{p_0}\right)^{R/C_p}\overline{\omega}\frac{\partial\overline{\theta}}{\partial p} + \left(\frac{p}{p_0}\right)^{R/C_p}\left[\nabla\cdot\overline{\mathbf{v}'\theta'} + \frac{\partial\left(\overline{\omega'\theta'}\right)}{\partial p}\right].$$

Here $\overline{\dot{Q}}(x,y,p,t)$ is the diagnosed monthly diabatic heating rate (K day^{-1}), $\mathbf{v}$ the horizontal wind vector, ω the pressure vertical velocity, and θ the potential temperature $[=T(p_0/p)^{R/C_p}]$. The overbar denotes the monthly mean, and the prime denotes the deviation of the 6-hourly analysis from this mean (i.e., the transient component). The transient component thus represents both synoptic and low-frequency (but submonthly) fluctuations.

Heating diagnosis from the ERA-15 and NCEP reanalyses was reported in Nigam et al. (2000), where intercomparison of ENSO heating structure was the focus. The heating diagnosed using analyzed and the mass-balanced ω was very similar in the ERA-15 case. The ERA-40 diagnosis was thus undertaken with the archived ω, that is, without any adjustments to this field. Except for the refined treatment of vector winds in high polar latitudes, the diagnosis technique is identical to that described in Nigam et al. (2000).[3]

The ERA-40 heating was diagnosed at the resolution of its NCAR data archive (i.e., on a 2.5° global horizontal grid and 23 pressure levels ranging from 1000 to 1 hPa), for the 1957–2002 period. Heating intercomparisons, all for the 1979–93 common period, are on a 2.5° latitude by 5° longitude grid.

4. Heating intercomparisons

a. Zonal mean

The integrated view—zonally and vertically—of the diabatic heating distribution is compared first, in Fig. 1. Shown is the full ERA-40 field, along with its *departure* from NCEP and ERA-15 counterparts. Both January and July ERA-40 heating contain a tropical heating maximum with the boreal summer maximum being particularly intense. In these maxima, resides the well-known intertropical coinvergence zone—the ascending branch of the meridionally divergent Hadley circulation. The ERA-40 departures are significant in both months but especially in July when they approach 50% of the full-field amplitude northward of the equator. The departures moreover mimic the full field structure (except in polar latitudes), indicating the diagnosed ERA-40 heating to be notably strong, especially in July when it is almost twice as large as NCEP heating.

The diagnoses are in greater accord in the winter subtropics, the Hadley cell descent region. Diabatic cooling in this region—of radiative origin—is no less impressive, but again the ERA-40 fields are stronger in both hemispheres, and more equatorward focused as well. Farther poleward, a secondary heating maximum is evident in the full fields, arising from the heat released along winter storm tracks. The ERA-40 and NCEP are in good agreement on this feature.

b. Zonal distribution

The heating distribution is, of course, far from being zonally uniform because of the presence of land surface and SST variations and orography. Surface inhomogeneities and their circulation influence organize heating, generating regional features such as the ITCZ, South Pacific convergence zone (SPCZ), Maritime Continent convection, Asian monsoon heating, and the subtropical

[3] The distinction between zonal and meridional wind is lost at the poles, where horizontal flow can only be meridional, dominated by the wavenumber 1 component. Zonal wind is thus set to zero and the meridional wind forced to be wavenumber 1 along the first off-polar grid row. In the earlier ERA-15 and NCEP heating diagnoses, the meridional wind was, incorrectly, set to zero instead, but with virtually no impact on heating estimates in the off-polar regions, as ascertained later.

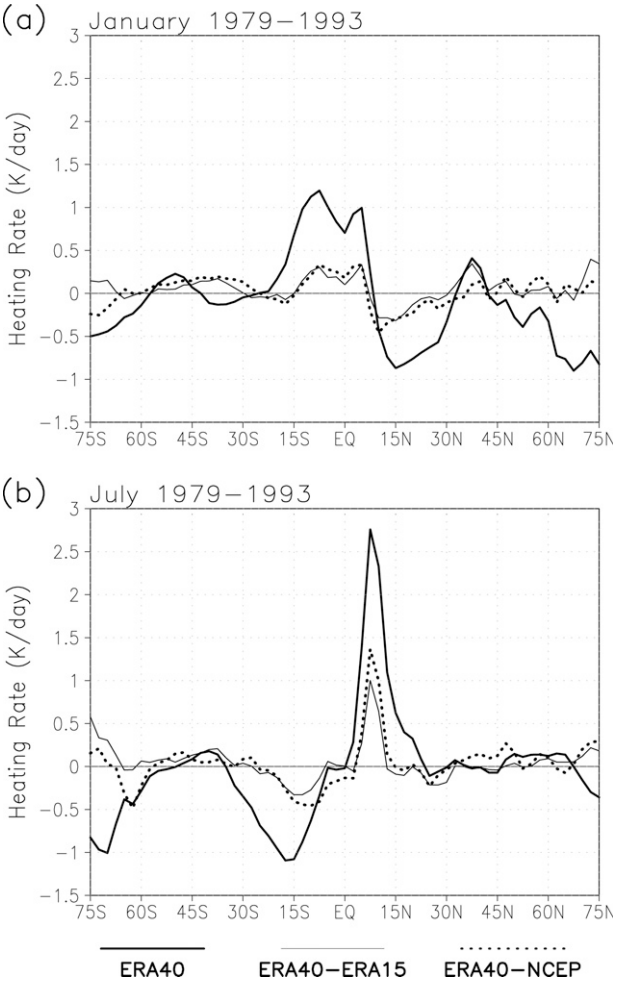

FIG. 1. Zonally and vertically averaged ERA-40 diabatic heating in (top) January and (bottom July) for the 1979–93 period climatology. Heating is residually diagnosed and the surface–125-hPa vertical average is mass weighted. The ERA-40 departure from the NCEP and ERA-15 diagnosed heating is also shown.

and eastern Pacific subsidence/descent and cooling zones, among others. These heating features, in turn, exert profound impact on the atmospheric general circulation.

The January and July ERA-40 heating distributions are shown in Figs. 2 and 3, respectively, along with the deviations from other heating fields. The ERA-40 heating is substantially stronger over the Maritime Continent and the eastern Pacific and Atlantic ITCZs in winter; for example, it is at least 50% larger than NCEP over the Maritime Continent. Consistent with stronger equatorial heating in most longitudes, ERA-40 exhibits stronger diabatic cooling in the off-equatorial latitudes, that is, a stronger Hadley cell. The winter cooling over midlatitude continents is, however, suppressed—notably over North America. The Atlantic storm track also extends more northward (into the Davis Strait) in ERA-40, as evident from the difference map.

The July differences (Figs. 3b,c) exhibit some of the same biases, but with heightened amplitude in the deep tropics, especially in the central/eastern basins. The ERA-40 heating in these ITCZ sectors is almost twice as strong as for NCEP, with attendant off-equatorial cooling biases in the winter hemisphere. The heating bias over the Asian and American monsoon regions is weaker but of the opposite sign, for example, the negative ERA-40 bias over the Indian subcontinent.

c. Hadley circulation

The zonal-mean distribution of ERA-40 heating is shown in Fig. 4 along with differences from the NCEP structure. The meridionally divergent circulation, comprising zonally averaged meridional and vertical velocities, is also shown in the same panels, using vectors. The ERA-40 heating in the deep tropics is stronger, especially in July, as seen in the earlier plots. The departure from NCEP heating (right panels)—the ERA-40 excess—is confined to the region above the planetary boundary layer in the Northern Hemisphere (NH) where its distribution mimics the climatological heating profile. The ERA-40 Hadley cells are, of course, clearly and consistently stronger. The midlatitude heating departures indicate the ERA-40 storm track heating to be weaker in boreal winter, but not at other times or in the other hemisphere.

d. Walker circulation

The October heating and divergent circulation is shown along the equator in the Pacific basin in Fig. 5. The divergent component of zonal wind and negative ω are plotted in the 5°S–5°N latitude band. The month of October was chosen as the SST contrast between the western and eastern basin is largest in this month on account of the fully fledged SST cold tongue in the eastern basin at this time. The divergent circulation is thus anticipated to be robust in this month. The ERA-40 plot shows one big clockwise cell over the Pacific—the Walker circulation—with strong rising motion over the Maritime Continent and weak sinking across the central and eastern Pacific basin. Narrow counterclockwise cells are evident at both ends of this big cell: the west one arising from the east–west symmetry of the Maritime Continent outflow and the east one from convection over equatorial South America, including Amazonia.

The ERA-40 Walker circulation is stronger than in NCEP, as indicated by the clockwise cell in the western/central basin in the difference map. The stronger divergent circulation in ERA-40 is, of course, consistent with its previously noted heating strength over the Maritime Continent in both summer and winter. The related strengthening of low-level descent over the central and eastern basin must lead to a stronger trade inversion in ERA-40. The counterclockwise cell to the east is, however,

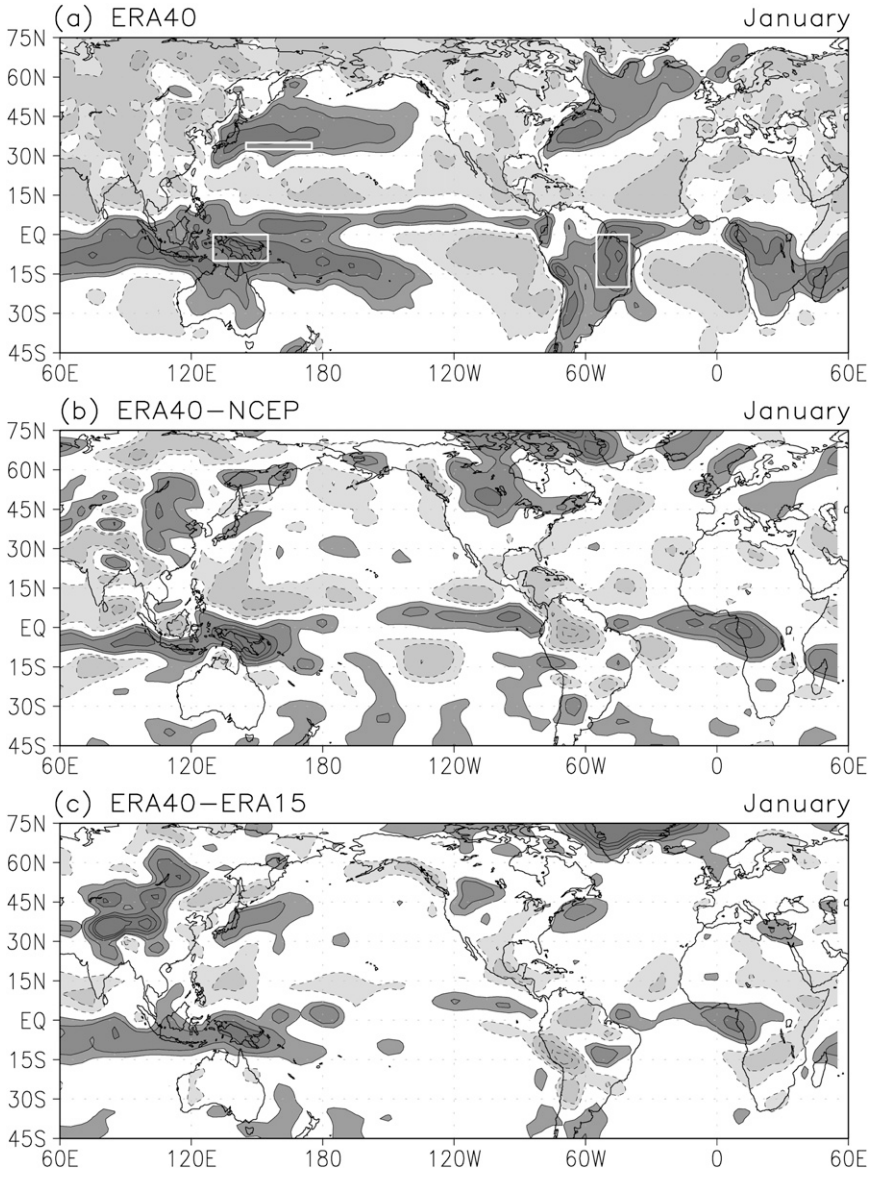

FIG. 2. (a) Vertically averaged ERA-40 diabatic heating in January for the 1979–93 period climatology. Heating is residually diagnosed and the surface–125 hPa vertical average is mass weighted. The ERA-40 departure from the (b) NCEP and (c) ERA-15 diagnosed heating are shown. The ERA-40 heating (a) is shown using the ±0.5, ±1.0, ±2.0, ±3.0, and ±4.0 K day^{-1} contours, while its *departure* is contoured at *half* these levels. Dark (light) shading indicates the diabatic heating (cooling) region; the zero contour is omitted in all panels.

weaker in ERA-40, reflecting less intense convection over equatorial South America vis-à-vis the NCEP reanalysis, as also in January (cf. Fig. 2b).

5. Tropical heating diagnosis: Inference from precipitation

Diabatic heating obtained from the ERA-40 circulation was found to be stronger in the tropics in both January and July (cf. Figs. 2 and 3). As both global reanalyses are constrained by similar (if not the same) large-scale circulation observations, which of the two heating diagnoses should be considered more reasonable? The dynamical consistency of 3D diabatic heating and the large-scale circulation can be a basis for this choice, but the involved diagnostic modeling (that yields the circulation response of specified heating; e.g., Nigam 1994) is not without its own caveats. Short of this exercise, a comparison of the

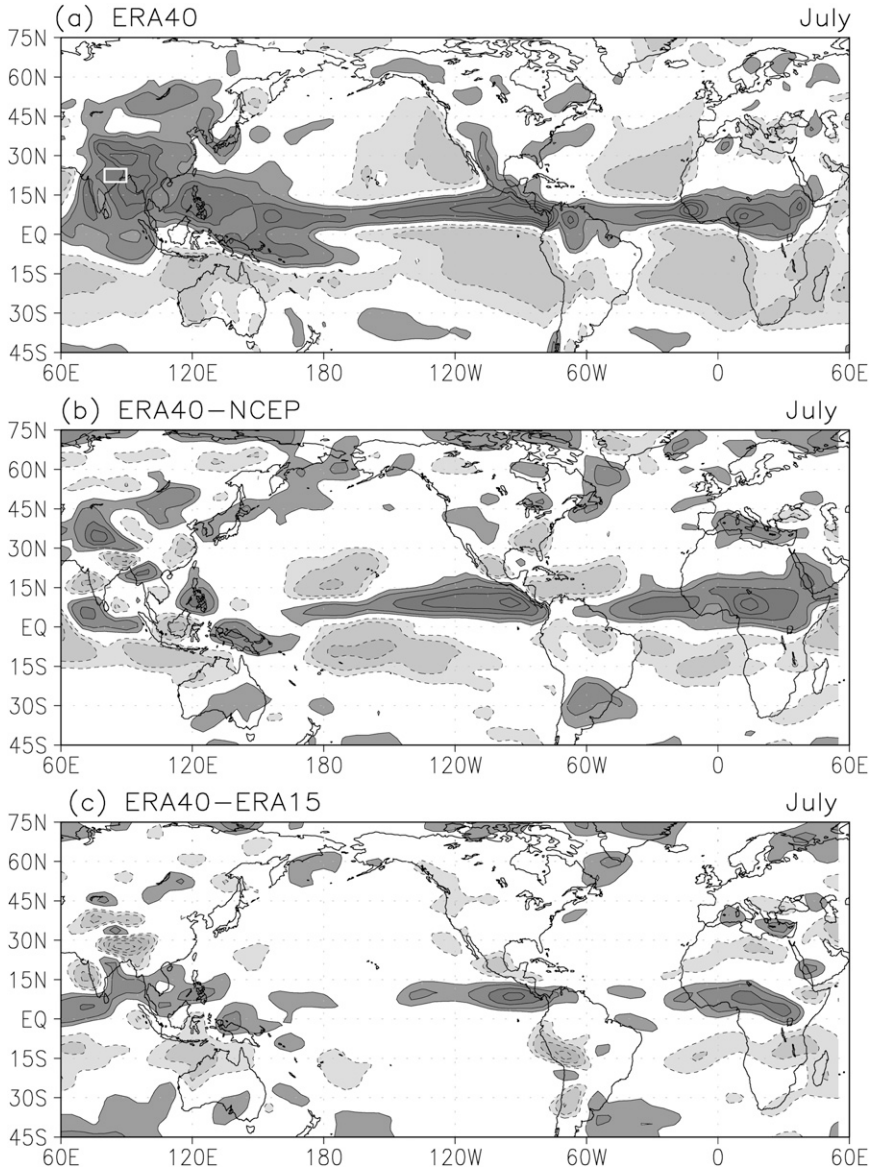

FIG. 3. As in Fig. 2 but for July.

heating structure and precipitation can be insightful, but only in regions where latent heating dominates, for example, the monsoon region and the deep tropics. The CMAP-2 precipitation rate (mm day^{-1}) is converted into the vertically averaged heating rate (K day^{-1}) by multiplying the former by $(gL\rho_w 10^{-5})/[C_p(P_s - 125)]$, where L is the latent heat of condensation (2.5×10^6 J kg^{-1}), g is gravity, ρ_w is the water density (10^3 kg m^{-3}), C_p is the specific heat of air at constant pressure (1004 J kg^{-1} K^{-1}), and P_s is surface pressure (hPa).

The monsoon region intercomparison is shown first, in Fig. 6. A Hovmöller plot of vertically averaged diabatic heating, additionally averaged across the eastern Indian subcontinent (80°–100°E), is displayed at monthly resolution. The comparison with precipitation is, of course, useful only in the rainy season.[4] More than amplitude, it is the monthly evolution of rainfall that provides discrimination between the competing heating diagnoses. From the perspective of northward migration of rainfall in the January–July period, the ERA-40 heating mimics CMAP rainfall evolution more closely than does

[4] Precipitation, by virtue of being positive definite, is of little corroborative value in other seasons (and regions) when (where) radiative cooling is dominant, as in winter over the Indian subcontinent.

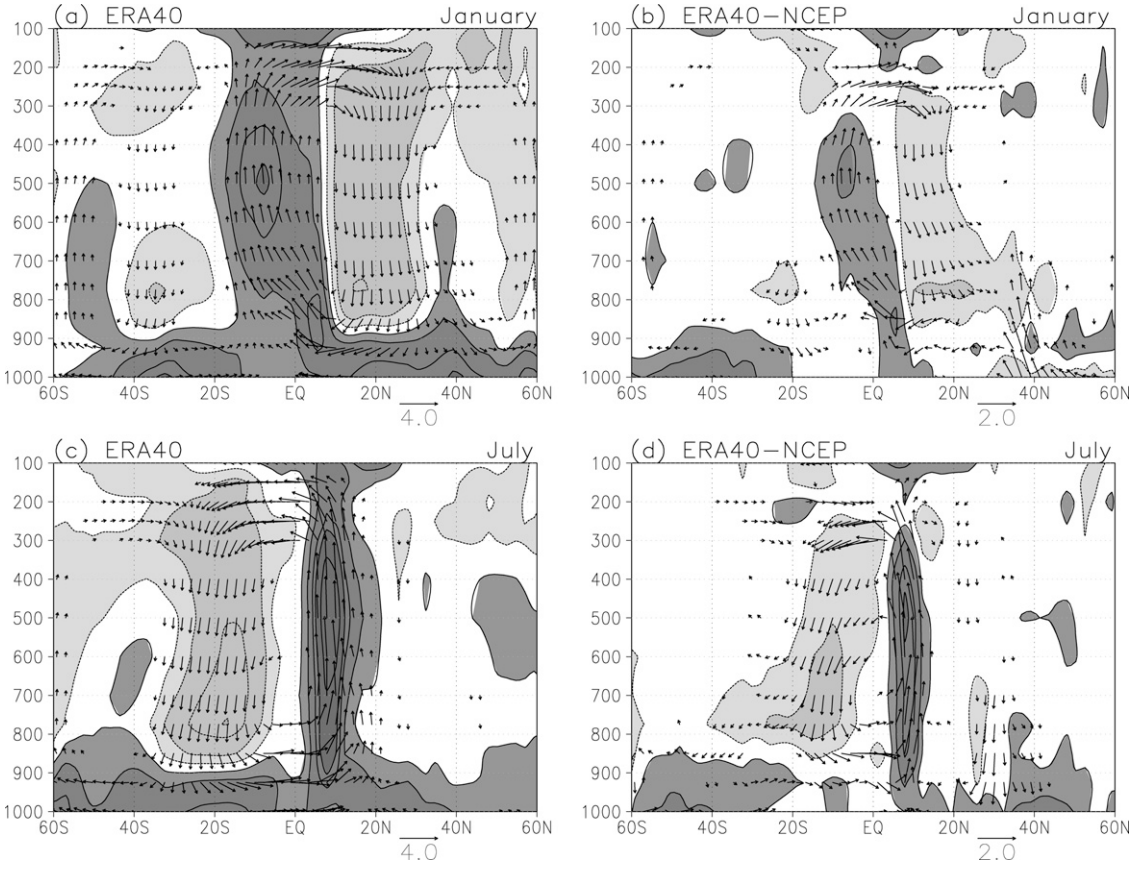

FIG. 4. Zonally averaged diabatic heating and the Hadley circulation for the ERA-40 reanalysis in (a) January and (c) July based on the 1979–93 period climatology; (b), (d) ERA-40 departures from the corresponding NCEP fields. Residual diabatic heating is contoured and shaded at the ±0.25, ±0.75, ±1.5, ±2.0, and ±3.0 K day^{-1} levels. Dark/light shading indicates the heating/cooling region. The Hadley circulation [zonal-mean v (m s^{-1}) and $-\omega$ (Pa min^{-1})] is displayed using vectors with the indicated scale; vectors smaller than 10% of the scale are not plotted. Note: vector scale for departures is half that of the full fields.

NCEP—likewise for the monsoon retreat. The south-of-the-equator location of the convection center in the nonmonsoon period is also more realistically captured in the ERA-40-based heating diagnosis. But the ERA-40 heating is a bit too strong, by ~0.5 mm day^{-1} (~15%) in the monsoon season, especially with respect to the CMAP-2 rainfall.

Heating evolution in the eastern tropical Pacific (140°–120°W) where heating diagnoses are far apart, especially in July (cf. Fig. 3b), is examined in Fig. 7. In this sector, the differences in diagnosed heating are not subtle and the choice of heating that is more in accord with observed precipitation (and large-scale circulation) is clear-cut: the ERA-40-based diagnosis. The CMAP-2 representation of the eastern Pacific ITCZ, including its northward summer migration and a hint of double-ITCZ structure in March–April, is mirrored in the ERA-40 heating structure. The heating amplitude, however, appears to be marginally excessive, as in the Indian monsoon sector.

6. Heating vertical structure: Intercomparison with TRMM profiles

The vertical distribution of heating is closely examined in the 1999–2001 period, when TRMM latent heating profiles are available as reference. The heating vertical structure is of some consequence in the tropics as circulation is sensitively dependent on the vertical gradient of heating (Q): The horizontal divergence ($-\partial\omega/\partial p$) is proportional to $\partial Q/\partial p$ in the tropics, linking the divergent circulation directly and the rotational circulation indirectly (through vortex stretching), with the vertical heating gradient. The heating vertical structure, to an extent, also reveals the convective–stratiform mix of precipitation, given the rather different characteristic heating profiles associated with the two convection processes (Houze 1997).

a. ITCZ heating

The heating vertical structure across the boreal winter ITCZ is examined first, in Fig. 8. The latent heating

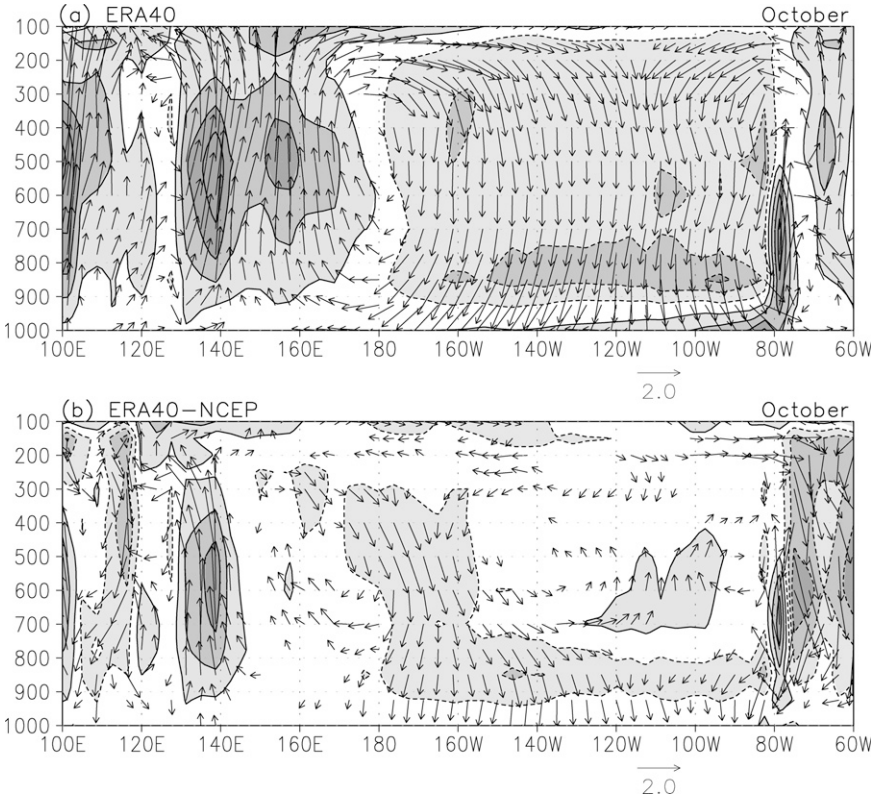

FIG. 5. (a) Diabatic heating and the Walker circulation in the ERA-40 reanalysis in October based on the 1979–93 period climatology. The 5°S–5°N latitudinal average is plotted in the calendar month of heightened zonal SST contrast, that is, when the SST cold tongue is fully fledged. (b) ERA-40 departures from the corresponding NCEP fields. Residual diabatic heating is contoured and shaded at the ±0.5, ±1.5, ±2.5, ±3.5, and ±4.5 K day^{-1} levels. Dark/light shading indicates the heating/cooling region, as before. The Walker circulation [divergent zonal wind (m s^{-1}) and $-\omega$ (Pa min^{-1})] is displayed using vectors with the indicated scale; vectors smaller than 20% of the scale are not plotted.

estimate from the TRMM CSH algorithm is shown along with NCEP model latent heating (generated from 6-h forecasts initialized by the reanalysis circulation) in the left panels. Residual diabatic heating from ERA-40, which includes radiative and sensible components as well, is displayed in the top right panel, while its NCEP counterpart from model forecasts is in the bottom right one. Immediately apparent is the striking zonal variation in the height of the latent heating maximum (left panels), in accord with Back and Bretherton's (2006) diagnosis of top-heavy convective heating profiles in the western equatorial Pacific and bottom-heavy ones in the eastern basin.

The NCEP model latent heating compares favorably with the TRMM estimate in the middle troposphere, with maximum heating (~3 K day^{-1}) at 400–500 hPa. Notable differences are however present at both upper and lower levels: The NCEP-model latent (and total) heating and, even more, the diagnosed ERA-40 heating extend too far up in the vertical—to the tropopause—at variance with the TRMM CSH structure. At lower levels, the NCEP model latent heating contains a secondary maximum (~1.5 K day^{-1}) in the central and eastern basin, while there is no hint of such feature in the TRMM heating. The discrepancy is likely related to the undersampling of shallow convection by the precipitation radar. Schumacher et al.'s (2007) diagnosis of heating vertical structure from sounding data collected during the TRMM Kwajalein experiment is, for example, more bottom-heavy than the corresponding radar inferred structure (see their Fig. 8 and related discussion).

A comparison of the NCEP model latent and total diabatic heating suggests the presence of pervasive radiative cooling (~1 K day^{-1}), which lowers the heating maximum in the western basin (to ~2 K day^{-1}) and leads to net cooling of the troposphere in the central/eastern basin, consistent with Johnson and Ciesielski's (2000) analysis of radiative cooling. The total model heating also does not contain the low-level structure present in latent heating, indicating offsets by the near-surface sensible heating and lower-troposphere radiative cooling. The

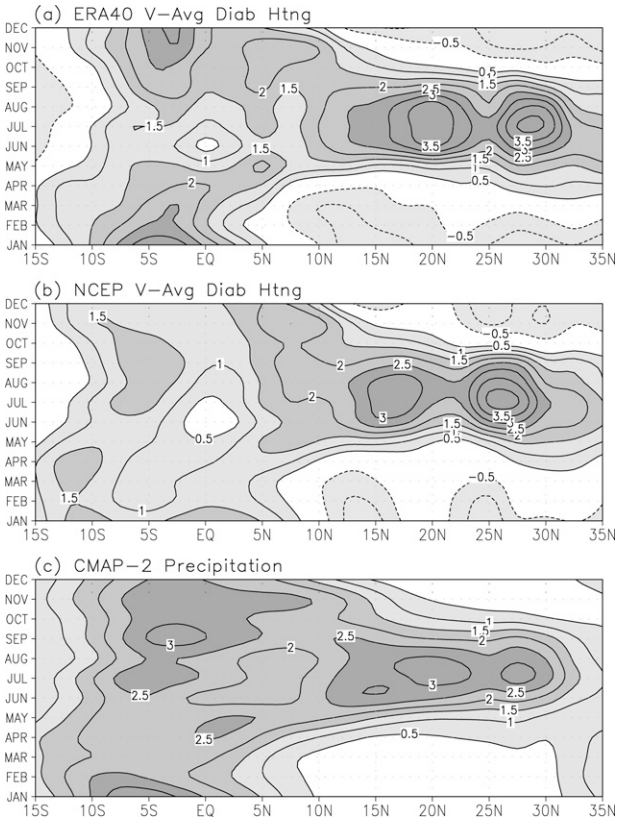

FIG. 6. Seasonal evolution of diabatic heating and precipitation over the Indian subcontinent sector (80°E–100°E) in the 1979–2002 climatology. Heating is residually diagnosed from global reanalyses and the mass-weighted surface–125-hPa vertical average is shown: (a) ERA-40; (b) NCEP; (c) CMAP-2 precipitation after its conversion into latent heating units. The contour interval and shading threshold is 0.5 K day^{-1} and the zero contour is omitted in all panels. Note: negative contours are present in upper panels as radiative (and sensible) heating is included there, on account of residual estimation.

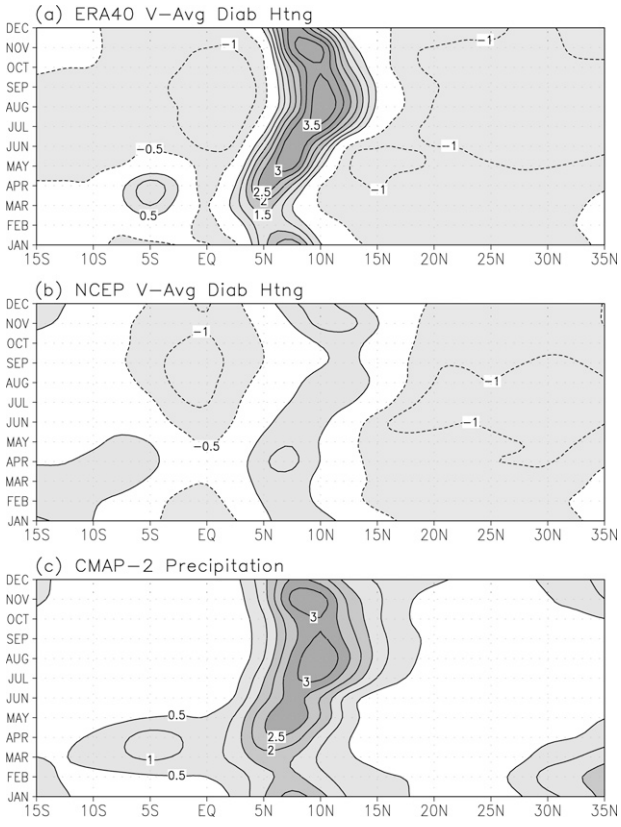

FIG. 7. As in Fig. 6 but for the eastern Pacific sector (140°–120°W).

ERA-40 residual heating differs from the NCEP model total heating principally in the strength and vertical extent of the western basin heating maximum, with the ERA-40 residual being stronger (by ~1 K day^{-1}).

b. Regional heating profiles

The heating vertical structure is closely compared in Fig. 9 by plotting the vertical profiles in four regions (two continental, one maritime land, and one oceanic): Indian summer monsoon (20°–25°N, 80°–90°E); South American convection (20°S–equator, 55°–40°W); Maritime Continent (10°S–equator, 130°–155°E); and winter storm tracks over the Pacific (32.5°–35°N, 145°–175°E). The first region is marked on Fig. 3 while the other three are outlined in Fig. 2. Since local maxima in the ERA-40 heating field are a basis for the choice of regions, there is potential for an implicit bias toward the ERA-40 profile being the strongest in the following intercomparisons. In addition to TRMM and the diagnosed ERA-40 and NCEP profiles, the NCEP model latent and total diabatic heating profiles are also shown. Note that TRMM provides a valuable reference, but not necessarily the validation target in the tropical plots, as it is itself produced in part from a model, albeit a cloud-resolving one which is no less immune to parameterization deficiencies.

1) INDIAN SUMMER MONSOON

The Indian summer monsoon heating profiles are plotted in Fig. 9a. The diagnosed heating profiles (black and green) exhibit remarkable agreement. The TRMM-CSH latent heating profile (red) is broadly similar but weaker than diagnosed heating everywhere, especially in the lower troposphere and near the tropopause. Some of the difference could be attributed to the implicit inclusion of sensible and radiative heating in the diagnosed profiles, except that the TRMM CSH profile is weaker. One normally expects total diabatic heating (e.g., residual heating) to be smaller than latent heating in the middle and upper troposphere in view of radiative cooling of the region (negative radiative heating). Such cooling is evident, for example, in the difference of the NCEP model's latent

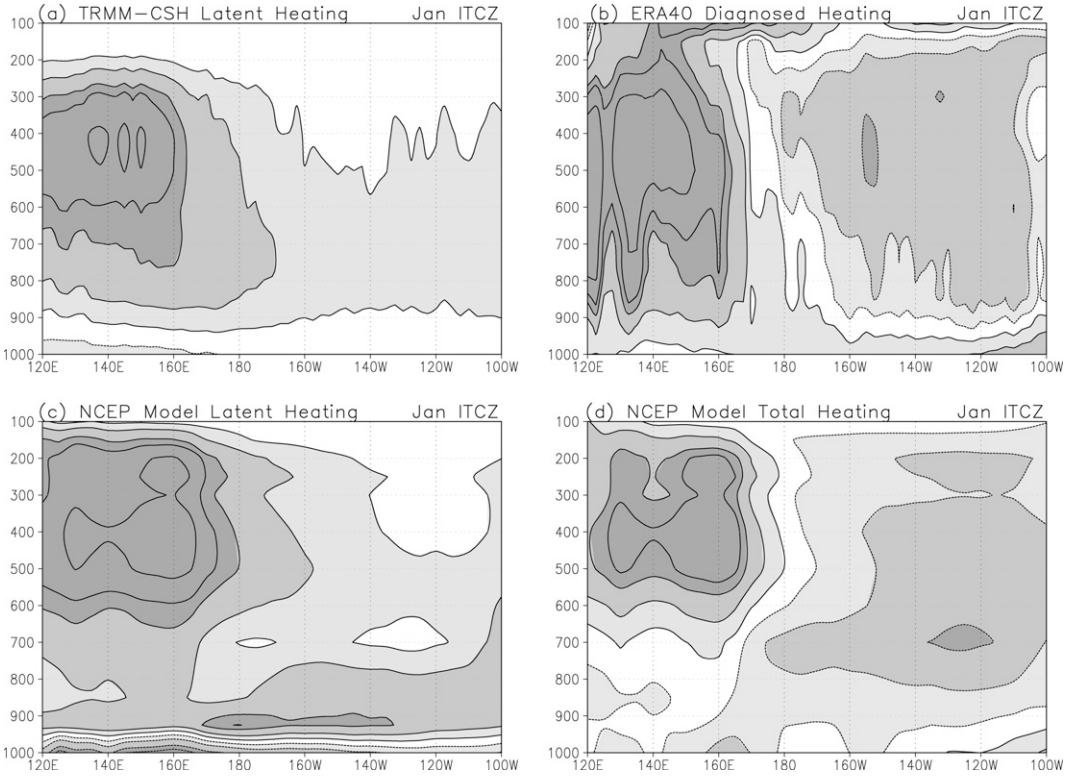

FIG. 8. Heating vertical structure in the ITCZ, based on 3-yr climatology (1999–2001); the overlapping data period. The equator–5°N latitudinal average in January is displayed: (a) TRMM-CSH latent heating, (b) ERA-40 diabatic heating (diagnosed), (c) NCEP-model latent heating, (d) NCEP-model total diabatic heating. Heating is contoured and shaded at ±0.25, ±0.75, ±1.5, ±2.0, and ±3.0 K day^{-1} levels, with the zero contour omitted, as before. Dark/light shading indicates the heating/cooling region.

(thin dashed red) and total (thin dashed green) heating profiles—a difference in line with Johnson and Ciesielski's (2000) radiative cooling estimate. The intercomparisons indicate TRMM CSH heating to be an underestimate (by up to 2 K day^{-1} in the lower troposphere!) and/or the residual ERA-40 and NCEP heating to be overestimates.

The aforementioned discrepancy is serious enough to merit further analysis. For instance, is there independent data that can help assess the competing heating diagnoses? Although assessment of the vertical structure is challenging, weighing in on the heating amplitude, especially of vertically integrated heating, is not. In the deep tropics, where latent heating dominates, the heating integral should equal the heat released in vapor condensation (at the rate of surface precipitation). The integral constraint is powerful but only where surface precipitation is well measured. The summer monsoon rainfall region over the Indian subcontinent may be one such region, having sufficient station data (e.g., Rajeevan et al. 2006).

The vertically integrated heating is converted into precipitation units (mm day^{-1}) to facilitate comparison with various station and satellite-based surface precipitation estimates in Table 1. The estimates range from 5.86 mm day^{-1} (TRMM CSH) to 12.90 mm day^{-1} (NCEP model latent), with the ERA-40 and NCEP-diagnosed heating-based precipitation close to the upper end of the range (~12.2 mm day^{-1}); IMD rainfall is 12.5 mm day^{-1} for reference. The large range results not from differences in the maximum heating rate (3.5–4.5 K day^{-1}) but from the spread in upper- and lower-troposphere heating rates. The overlap of the diagnosed heating profiles is quite reassuring in this regard, but the lack of internal consistency between the TRMM-CSH model–based precipitation (5.86 mm day^{-1}) and the constraining TRMM 3A25 precipitation retrieval (8.55 mm day^{-1}) and other TRMM retrievals [3B43 (10.92 mm day^{-1}) and the experimental 3A12 (7.57 mm day^{-1})] is worrisome. Station precipitation analyses over this part of the subcontinent are unfortunately not in accord either, with CRU (8.22) and IMD (12.50) estimates being ~50% apart. The 1979–2001 CRU and IMD summer rainfall climatologies do not exhibit such discrepancy, though.

The spread in station and satellite analyses notwithstanding, our assessment indicates the TRMM-CSH-based precipitation estimate to be an outlier—on the low

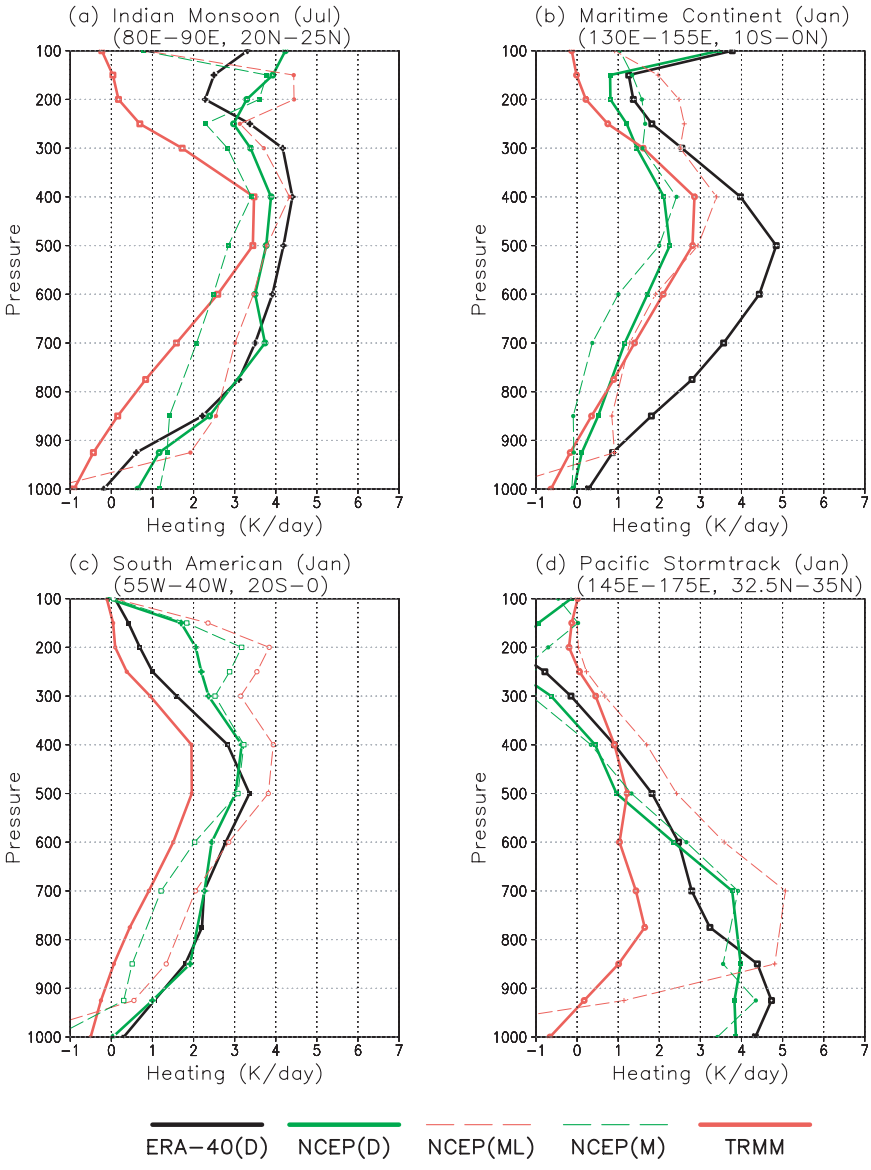

FIG. 9. Diabatic heating profiles in selected region marked in Figs. 2 and 3: (a) Indian summer monsoon (July, land box); (b) Maritime Continent (January, land box); (c) South American continent (January, land box); and (d) Pacific winter storm tracks (January, oceanic box). Five profiles are shown in each case: Diagnosed ERA-40 (thick black) and NCEP (thick green) heating; NCEP-model latent (thin red dashed) and total diabatic (thin green dashed) heating; and the TRMM-CSH latent heating profile (thick red). All profiles are for the 1999–2001 period.

side—at least over this Indian subcontinent region. The conclusion is supported by TRMM's own precipitation retrievals and station observations. It is presently unclear if the underestimation results from CSH heating profile's shape or weak amplitude (or both).

2) MARITIME CONTINENT

The heating vertical structure over the western end of the SPCZ (cf. Fig. 2a) is examined in the top right panel of Fig. 9. Heating profiles are displayed for January when convection is most intense in this region (and over northern Australia, the peak phase of the Australian monsoon). The profiles are in remarkable agreement except for the ERA-40 profile, which is much too strong in the middle and lower troposphere. The Table 1 precipitation intercomparison supports this assessment: satellite-based estimates are in the 7–9 mm day^{-1} range, that is, just shy of the CRU station precipitation (9.18 mm day). The precipitation rate

implied by the residual ERA-40 heating profile, on the other hand, is 11.22 mm day^{-1}, that is, about 25% larger. The diagnosed ERA-40 heating thus seems excessive and indicative of an overly strong divergent circulation in the deep tropics in ERA-40 reanalysis (see also Figs. 4a,b).

3) South American continent

Heating profiles over the major continental convection center in austral summer—eastern tropical South America—are shown in the bottom left panel of Fig. 9. One finds interesting parallels with the boreal summer continental convection case (Indian monsoon) examined earlier: remarkable similarity of the ERA-40 and NCEP diagnosed heating profiles, with both being larger than TRMM CSH heating at every level, but especially in the lower troposphere. The station and satellite precipitation analysis are in good agreement here (cf. Table 1), all being in the 6.5–7.5 mm day^{-1} range, except for the 3A25 estimate (~4.7 mm day^{-1}). The implied precipitation rate from the ERA-40 heating diagnosis also comes in at 7.70 mm day^{-1}. Against this backdrop of rare accord among observational estimates, the TRMM-CSH-based precipitation rate (3.31 mm day^{-1}) stands out as an outlier on the low side (by up to 50%), much as in the Indian summer monsoon case.

4) Pacific winter storm tracks

Heating profiles in an oceanic midlatitude region where winter precipitation is of stratiform origin are shown in Fig. 9d. The region stands out for exhibiting remarkable agreement, not only among the diagnosed heating profiles but also between them and the NCEP-model total heating. The latter agreement, in particular, gives credence to the NCEP-model latent heating distribution, making it a reasonable target for the TRMM-CSH latent heating profile. The availability and credibility of the NCEP latent heating offers unique opportunities for assessing TRMM CSH latent heating in the subtropics and midlatitudes where surface precipitation cannot be used for evaluation of competing heating diagnoses, in view of substantial sensible and radiative heating contributions to total diabatic heating here. The very large difference (~100%) between the TRMM-CSH and NCEP-model latent heating, while noteworthy, is not altogether surprising as the CSH algorithm is based on the cumulus ensemble model simulations of convective clusters with stratiform anvil upper-level heating and, as such, is not well suited for modeling precipitation processes associated with the more common frontal lifting in the subtropics and midlatitudes. The closeness of the 3A25 precipitation retrieval (which constrains the CSH algorithm) and precipitation rates implied by the ERA-40 diagnosed heating and NCEP model latent heating (cf. Table 1) supports this assertion.

TABLE 1. Estimated precipitation in four geographical regions during the 1999–2001 period. Estimates (mm day^{-1}) are obtained from the vertical integral of diagnosed heating profiles, cloud ensemble simulations and global model forecasts, satellite observations, and station data. The smallest estimate for each region is indicated in bold.

Precipitation from diagnosed total diabatic heating		Precipitation from model heating			Precipitation retrieved from satellite observations				Precipitation from land station observations	
ERA-40	NCEP	TRMM-CSH latent (expt analysis)	NCEP model total	NCEP model latent	CMAP-2	TRMM 3B43 TMI, PR, gauge (expt analysis)	TRMM 3A12 TMI (expt analysis)	TRMM 3A25 PR (expt analysis)	CRU TS2.1	IMD
				Indian monsoon region (20°–25°N, 80°–90°E) July						
12.31	12.23	**5.86**	9.47	12.90	10.65	10.92	7.57	8.55	8.22	12.50
				Maritime Continent (10°S–equator, 130°–155°E) January						
11.22	4.84	5.15	**4.14**	7.74	9.17	8.09	7.10	6.82	9.18	
				South American region (20°S–equator, 55°–40°W) January						
7.70	8.69	**3.31**	7.45	10.10	6.79	6.83	6.98	4.67	7.52	
				Pacific storm tracks region (32.5°–35°N, 145°–175°E) January						
7.69	6.97	**2.88**	7.40	8.33	5.58	6.37	5.01	7.44		

7. Concluding remarks

Diabatic heating is a very influential but elusive quantity. It exerts a profound influence on the atmospheric general circulation, which in turn modulates the heating distribution. The heating vertical structure, in particular, is of some consequence for atmosphere–ocean interaction in the tropics and atmosphere–land surface interactions in the subtropics. Diabatic heating is generated principally from the latent heat release during atmospheric convection. Modeling of convection, especially partitioning between convective and stratiform processes, remains a formidable challenge, compromising the diabatic heating distributions generated in atmospheric models (e.g., Nigam et al. 2000).

The refined estimates of 3D heating presented here are based on consistency with the large-scale postprocessed circulation and should spur improvements in convection parameterizations. The heating diagnosis should ideally be conducted using data on the assimilating model's native grid to preclude interpolation errors from corrupting the residual estimation (e.g., Trenberth et al. 2002). Such distortions are, however, expected to be small given the high vertical resolution (23 levels) of the ERA-40 postprocessed data. (Trenberth et al. suggest 30 levels to be sufficient for avoidance of interpolation related errors.) Regardless, inter-reanalysis differences are of greater concern in the tropics—the primary analysis domain here.

Diabatic heating, interestingly, is not part of the publicly accessible ERA-40 data archive, despite its wide use in climate diagnostics. The diabatic heating generated during the reanalysis cycle, as part of the short-term bridging forecast, would be useful even though its consistency with the large-scale reanalysis circulation is not assured, given the influence of the physical parameterization schemes during the bridging forecast period. For these and other reasons, diabatic heating was residually diagnosed from the ERA-40 circulation and compared with heating distributions obtained similarly from the NCEP and ERA-15 reanalyses and with the TRMM CSH heating.

The present study is also motivated by the need to confront the TRMM diagnosis of latent heating structure, based on *local* retrievals of surface convective and stratiform rain rates and *local* convective and stratiform heating profiles from the Goddard cumulus ensemble model, with the heating vertical structure based on *large-scale* circulation (assimilated in reanalysis), evaluating both in the process. The evaluation is especially valuable as the TRMM-based diagnosis of heating vertical structure is considered an experimental product on less certain footing than the corresponding satellite-based retrievals of surface precipitation.

We find the following:

- ERA-40 residual heating in the tropics is stronger than NCEP's (and ERA-15), especially in July when its zonal–vertical average is twice as large. The bias relative to NCEP is strongest over the Maritime Continent in January and over the eastern basins and Africa in July, and is reflected in the vigor of the divergent Hadley and Walker circulations and in enhanced diabatic cooling of the off-equatorial descent regions.
- Another notable bias relative to NCEP is the suppressed winter cooling of the midlatitude continents in the ERA-40 residual heating, by $\sim$0.5 K day^{-1}.
- Comparison of seasonal precipitation and vertically averaged heating evolutions shows ERA-40 heating to be much more realistic than NCEP's over the eastern tropical Pacific, albeit a bit excessive.

The ERA-40 and NCEP residual heating profiles are finally compared with the TRMM-CSH latent heating profile and NCEP-model heating profiles in four regions of heavy precipitation: Indian summer monsoon, South American convection, Maritime Continent, and winter storm tracks over the North Pacific. Intercomparison of precipitation estimates from heating profile integrals and station and satellite analyses during the overlapping data period (1999–2001) provides a basis for assessment of the heating products (cf. Table 1), assuming confidence in the station precipitation datasets. We find the following:

- TRMM CSH latent heating is generally weak, by as much as a factor of 2—a low-side outlier among nine precipitation estimates in three of the four analyzed regions!
- The vertical integral of the CSH latent heating profile in the tropics is inconsistent with the TRMM rainfall retrievals constraining the CSH algorithm (e.g., the 3A25 analysis).

More regionally and specifically, we find the following:

- Monsoon heating profiles over eastern India are remarkably similar in the ERA-40 and NCEP residual diagnoses, with vertically integrated heating of $\sim$12 mm day^{-1}. The TRMM CSH profile is weak at all levels, with a $\sim$6 mm day^{-1} integral. Station analyses, unfortunately, have large spread: $\sim$8 mm day^{-1} (CRU) and $\sim$12 mm day^{-1} (IMD); with CMAP-2 in between ($\sim$10.5 mm day^{-1}). The station–satellite spread notwithstanding, TRMM CSH heating is strongly underestimated and the ERA-40 and NCEP residual heating fairly accurate here.
- The Maritime Continent heating profile in the NCEP residual diagnosis and TRMM CSH heating are quite similar, with vertical integrals of $\sim$5 mm day^{-1}. The ERA-40 residual heating is almost twice as strong here, with an integral of $\sim$11 mm day^{-1}. Comparison with CRU and CMAP-2 rainfall (both $\sim$9 mm day^{-1}), however, shows ERA-40 heating to be excessive and the TRMM CSH and NCEP heating to be too weak.
- Diagnosed heating profiles over eastern tropical South America are in remarkable agreement, much as over

eastern India. The implied rainfall (~8 mm day^{-1}) is moreover in agreement with the station–satellite rainfall estimates (~7 mm day^{-1}). Against this backdrop of rare accord, the TRMM-CSH heating integral stands out—at 3.3 mm day^{-1}, that is, 50% smaller—with the profile amplitude, rather than shape, being the cause of the discrepancy.

The TRMM CSH algorithm clearly needs to be evaluated more thoroughly across more regions and seasons. The evaluation must include close intercomparisons with 3D diabatic heating diagnosed from the *large-scale* circulation (the component assimilated in current global reanalysis); and new station precipitation data over the oceans, for example, the Tropical Ocean and Global Atmosphere–Tropical Atmosphere Ocean (TOGA–TAO) array rainfall measurements in the eastern tropical Pacific.

Acknowledgments. We thank Anthony Del Genio, editor, for insightful review and advice, and the two anonymous reviewers for their constructive remarks. Steven Chan was supported by the NASA Earth System Science Fellowship (2004-2007). Sumant Nigam acknowledges NOAA and NSF support through CPPA-NA17EC1483 and ATM-0649666 grants. Both thank Renu Joseph, Alfredo Ruiz-Barradas, and Hezekiah Carty for help with data sets and analysis.

REFERENCES

Andersson, E., and Coauthors, 2005: Assimilation and modeling of the atmospheric hydrological cycle in the ECMWF forecasting system. *Bull. Amer. Meteor. Soc.,* **86,** 387–402.

Back, L. E., and C. S. Bretherton, 2006: Geographic variability in the export of moist static energy and vertical motion profiles in the tropical Pacific. *Geophys. Res. Lett.,* **33,** L17810, doi:10.1029/2006GL026672.

Ebisuzaki, W., 1996: Consistency of the diabatic heating in the NMC/NCAR reanalysis. *Proc. 20th Climate Diagnostic Workshop,* Seattle, WA, NOAA/Climate Prediction Center, 232–234.

Gibson, J. K., P. Kållberg, S. Uppala, A. Hernandez, A. Nomura, and E. Serrano, 1997: ERA-15 description. ERA-15 Project Rep. Series No. 1, ECMWF, 84 pp.

Holopainen, E., and C. Fortelius, 1986: Accuracy of estimates of atmospheric large-scale energy flux divergence. *Mon. Wea. Rev.,* **114,** 1910–1921.

Hoskins, B. J., H. H. Hsu, I. N. James, M. Masutani, P. D. Sardeshmukh, and G. H. White, 1989: Diagnostics of the global atmospheric circulation based on ECMWF analyses 1979–1989. WCRP-27, WMO/TD-No. 326, World Meteorological Organization, 217 pp.

Houze, R. A., 1997: Stratiform precipitation in regions of convection: A meteorological paradox. *Bull. Amer. Meteor. Soc.,* **78,** 2179–2196.

Johnson, R. H., and P. E. Ciesielski, 2000: Rainfall and radiative heating rates from TOGA COARE atmospheric budgets. *J. Atmos. Sci.,* **57,** 1497–1514.

Kållberg, P., P. Berrisford, B. Hoskins, A. Simmons, S. Uppala, S. Lamy-Thépaut, and R. Hine, 2005: ERA-40 atlas. ERA-40 Project Rep. Series 19, 191 pp. [Available online at http://www.ecmwf.int/research/era/ERA-40_Atlas/docs/index.html.]

Kalnay, E., and Coauthors, 1996: The NCEP/NCAR 40-Year Reanalysis Project. *Bull. Amer. Meteor. Soc.*, **77,** 437–471.

Mesinger, F., and Coauthors, 2006: North American Regional Reanalysis. *Bull. Amer. Meteor. Soc.*, **87,** 343–360.

Mitchell, T. D., and P. D. Jones, 2005: An improved method of constructing database of monthly climate observations and associated high-resolution grids. *Int. J. Climatol.,* **25,** 693–712.

Nigam, S., 1994: On the dynamical basis for the Asian summer monsoon rainfall—El Niño relationship. *J. Climate,* **7,** 1750–1771.

——, C. Chung, and E. DeWeaver, 2000: ENSO diabatic heating in ECMWF and NCEP reanalyses, and NCAR CCM3 simulation. *J. Climate,* **13,** 3152–3171.

Pan, H.-L., and W. S. Wu, 1994: Implementing a mass flux convective parameterization package for the NMC medium-range forecast model. Preprints, *10th Conf. on Numerical Weather Prediction,* Portland, OR, Amer. Meteor. Soc., 96–98.

Rajeevan, M., J. Bhate, J. D. Kale, and B. Lal, 2006: A high resolution daily gridded rainfall data for Indian region: Analysis of break and active monsoon spells. *Curr. Sci.,* **91,** 296–306.

Schumacher, C., R. A. Houze, and I. Kraucunas, 2004: The tropical dynamical response to latent heating estimates derived from TRMM precipitation radar. *J. Atmos. Sci.,* **61,** 1341–1358.

——, M. H. Zhang, and P. E. Ciesielski, 2007: Heating structures of the TRMM field campaigns. *J. Atmos. Sci.,* **64,** 2593–2610.

Tao, W.-K., S. Lang, J. Simpson, and R. Adler, 1993: Retrieval algorithms for estimating the vertical profiles of latent heat release: Their applications for TRMM. *J. Meteor. Soc. Japan,* **71,** 685–700.

——, and Coauthors, 2001: Retrieved vertical profiles of latent heat release using TRMM rainfall products for February 1998. *J. Appl. Meteor.,* **40,** 957–982.

Tiedtke, M., 1989: A comprehensive mass flux scheme for cumulus parameterization models. *Mon. Wea. Rev.,* **117,** 1779–1800.

——, 1993: Representation of clouds in large-scale models. *Mon. Wea. Rev.,* **121,** 3040–3061.

Ting, M., and P. D. Sardeshmukh, 1993: Factors determining the extratropical responses to equatorial diabatic heating anomalies. *J. Atmos. Sci.,* **50,** 907–918.

Trenberth, K. E., D. P. Stepaniak, J. W. Hurrell, and M. Fiorino, 2001: Quality of reanalyses in the tropics. *J. Climate,* **14,** 1499–1510.

——, ——, and J. Caron, 2002: Accuracy of atmospheric energy budgets from reanalyses. *J. Climate,* **15,** 3343–3360.

Uppala, S., and Coauthors, 2005: The ERA-40 Re-Analysis. *Quart. J. Roy. Meteor. Soc.,* **131,** 2961–3012.

White, G., and S. Saha, 1996: Three-dimensional diabatic heating fields from the NCEP/NCAR reanalysis. *Proc. 20th Climate Diagnostic Workshop,* Seattle, WA, NOAA/Climate Prediction Center, 284–287.

Xie, P., and P. Arkin, 1996: Analyses of global monthly precipitation using gauge observations, satellite estimates, and numerical model predictions. *J. Climate,* **9,** 840–858.

Yanai, M., and T. Tomita, 1998: Seasonal and interannual variability of atmospheric heat sources and moisture sinks as determined from NCEP–NCAR Reanalysis. *J. Climate,* **11,** 463–482.